Vortex-induced vibrations of a freely vibrating cylinder near a plane boundary: Experimental investigation and theoretical modelling

De Oliveira Barbosa, Joao; Qu, Yang; Metrikine, Andrei; Lourens, Eliz-Mari

DOI
10.1016/j.jfluidstructs.2017.01.002

Publication date
2017

Document Version
Accepted author manuscript

Published in
Journal of Fluids and Structures

Vortex-induced vibrations of a freely vibrating cylinder near a plane boundary: experimental investigation and theoretical modelling

by
João Barbosa*+
Yang Qu*
Andrei Metrikine*
Eliz-Mari Lourens*

Abstract

This work reports on experiments that were performed with a freely vibrating cylinder exposed to currents and placed near a plane boundary parallel to the cylinder axis. It is observed that the proximity of the boundary affects the vertical response of the cylinder in two ways: (i) for gaps between 0.75 and 2 diameters (D), the amplitude of oscillation is reduced; (ii) for gaps smaller than 0.75D, the cylinder impacts the boundary, resulting in an increase of amplitudes and frequencies of oscillations as the flow is accelerated. The in-line force acting on the cylinder is also examined, and the dependency of its harmonic components on the flow velocity and distance to the boundary is evaluated. Besides the typical amplification of the mean component inside the lock-in region, it is also observed that as the cylinder is placed closer to the boundary, the harmonic component with the frequency of the vertical oscillations increases, while the component with twice that frequency decreases in similar amount.

Based on the experimental observations, an existing wake-oscillator model for vortex-induced vibrations is enhanced in order to account for the effect of the boundary. The proposed model introduces an effective damper that is activated when the cylinder reaches a certain distance from the boundary, and a damper/spring set representing the rigidity of the boundary and the dissipation of energy due to impact.

Keywords: vortex-induced vibrations; fluid-structure interaction; wake-oscillator

1. Introduction

As a fluid flows past a stationary cylindrical body, vortices are shed alternately from its upper and lower parts. The cylinder is consequently subjected to cross-flow (lift) forces at the vortex shedding frequency, and in-line forces that are characterized by a mean and a harmonic component at twice the shedding frequency. If the cylinder is free to move, amplifications of its response may occur when the shedding frequency approaches and subsequently locks onto the cylinder's natural frequency. This amplification of the vortex-induced vibrations (VIV) has been investigated since the second half of the 20th century, and reports on several experimental works can be found in literature [1-10]. Based on the presented results, some simple models for the prediction of the flow-induced response of cylinders have been constructed.

A great number of the experiments on VIV deal with a rigid cylinder submerged in water and subjected to a steady flow. These types of experiments can be divided into three distinct groups: (i) stationary experiments, in which the cylinder is fixed and the acting forces are measured [1]; (ii) forced vibration experiments, in which an immersed cylinder is forced to move with a given amplitude and frequency, and the fluid forces are registered [2,3]; and (iii) free vibration experiments, in which a cylinder can vibrate freely in the flow, and its motion is recorded [3-10].

The first type of experiment aims at characterizing the fluid forces acting on very stiff structures, such as bridge piers. Knowing these forces, the stability of the supports can be assessed.

The goal of the second type of experiment is to quantify the components of the fluid forces that are in phase with the velocity (resulting in an added damping) and in phase with the acceleration (resulting in an added mass), for a wide range of amplitudes and frequencies of the cylinder's motion. The steady-state response of a general cylindrical structure can thereafter be estimated by finding the amplitude-frequency pair whose corresponding

* Affiliation: TU Delft, Stevinweg 1, 2628 CN Delft, Netherlands
+ Corresponding author: +31 15 278 2732, J.M.DeOliveiraBarbosa@tudelft.nl

force components (added mass and added damping) satisfy the structural equation of motion. The assumption of single frequency response is however inadequate for flexible structures, where travelling waves with different frequencies can co-exist.

During the third type of experiments, namely free vibration experiments, the amplitudes and frequencies of the cylinder's motion are recorded and subsequently used to tune empirical models that simulate the fluid-structure interaction, such as the wake-oscillator model [11,12]. No assumptions are made about the frequency of the response, but the characteristics of the measured vibrations are dependent on parameters such as the mass of the cylinder and the damping in the supports. Hence, the usability of a given set of results is limited to conditions similar to those in the experimental scenario.

Important observations from the mentioned experiments are:

- For stationary cylinders, the vortex shedding frequency f_s is proportional to the flow velocity V and inversely proportional to the diameter of the cylinder D. The relation between these variables is

$$f_s = \mathrm{St}\frac{V}{D} \tag{1}$$

  where St is the Strouhal number (in the subcritical flow regime, $\mathrm{St} \approx 0.2$).
- For freely vibrating cylinders, there is a range of flow velocities where the vortex shedding frequency remains close to the natural frequency of the cylinder f_n. In this range of velocities, termed the lock-in region, the oscillation amplitude is increased. Lock-in is, in most cases, limited to $4 < V_\mathrm{r} < 10$, where V_r is the reduced flow velocity, defined as

$$V_\mathrm{r} = \frac{V}{f_n D}. \tag{2}$$

- The lock-in region can be divided into two parts, one where the amplitude of oscillation is about $1.2D$ (for $4 < V_\mathrm{r} < 6$), and one where the oscillation amplitudes are about $0.6D$ (for $V_\mathrm{r} > 6$). The mentioned limits are approximate. Outside the lock-in region, the vortex shedding frequency is approximately the same as the shedding frequency for stationary cylinders f_s, defined in eq. (1).
- For the forced vibration experiments, there are some frequency-amplitude combinations for which the fluid forces in phase with the cylinder velocity are in the same direction as the cylinder's motion: the so-called negative added damping. This means that the flow transfers energy to the cylinder instead of damping its motion. These frequency-amplitude combinations correspond to the lock-in ranges observed in the free vibrations.

In all of the above-mentioned experiments, the cylinders are placed at a sufficiently large distance from the bottom of the testing flume (or wind tunnel), so that the boundary does not influence the observed phenomena. If the cylinder is placed sufficiently close to the boundary, the fluid-cylinder interaction starts to be affected by the boundary in two ways: firstly, the flow pattern is altered because the fluid finds resistance when going through the gap between the cylinder and the boundary; secondly, the possible collision of the cylinder with the bottom changes the natural frequency of the system and introduces impact forces.

There are a number of publications on experiments aimed at studying the effect of a boundary on the fluid-structure interaction forces for the case of stationary cylinders [13-18]. Important conclusions of these studies are that vortex shedding is suppressed for gaps smaller than one third of the cylinder's diameter, and that there is a mean cross-flow force that pushes the cylinder away from the boundary. Experiments that consider free or forced vibrations of a cylinder near a plane wall are more rare [19-20]. Nevertheless, an important conclusion is that also for small gaps (even smaller than $0.3D$), VIV can occur. This conclusion implies that the motion of the cylinder stimulates vortex shedding, a phenomenon that is suppressed in cases where the cylinder is fixed.

In this contribution, the results obtained during stationary and free vibration experiments for assessing the influence of a near boundary are reported. The motivation for the experiments was the scarcity of reports on freely vibrating cylinders near a plane wall. The obtained dataset provides further insight in the behaviour of cylindrical structures located near a boundary, such as pipelines or power cables on the seabed, thus allowing for more accurate predictions of the dynamic behaviour of such systems. Based on the experimental results, an extended wake-oscillator model [11,12] capable of representing the boundary effects is proposed. Section 2 describes the experimental setup, section 3 reports on the results from the stationary experiments, section 4 on

the results from the free vibration experiments, and section 5 describes how the observed dynamics can be incorporated into the wake-oscillator model (based on the Van der Pol equation). Conclusions are summarized in section 6.

2. Experimental setup

The stationary and free vibration experiments were conducted at the Water Lab of TU Delft, in the Kantelgoot 1 flume. The flume is 14.5m long, 0.40m wide, the maximum water depth is 0.45m, and the maximum allowed discharge is 85l/s. During the experiments, the water depth was kept constant at $d = 0.40$ m. The section chosen for the experiment was 8m downstream from the inlet, where it was expected that the flow had already stabilized.

Figure 1a-c shows the assembled setup and its schematization for the stationary and free vibrations layouts. An outer frame, composed of two vertical poles and one horizontal beam, is fixed to the sides of the flume. Then, an aluminium inner frame, composed of two vertical beams, one top beam and a lower cylinder, is connected to the outer frame. The horizontal connection is established through "frictionless" rollers (which allow the vertical motion of the inner frame) and load cells (used to measure the in-line forces: for the stationary experiments, one load cell is used on each side, while for the free vibration experiments, two load cells are used on each side). The vertical connection is achieved through two load cells that measure in-line and cross-flow forces (stationary experiments) or through springs sets (free vibration experiments). The position of the upper beam can be adjusted so that the gap between the bottom of the flume and the cylinder can assume different values.

The outer frame is made rigid and serves as support for the inner frame, which is the one being monitored. Figure 1d,e show the schematization of the inner frame and the forces that are measured for the stationary and free-vibration experiments, respectively.

The loads cells used in the experiment are a product of the company SCAIME [21]. Load cells with a maximum capacity of 10kg (AL10C3SH5E) were used to measure the in-line forces, while one load cell of 30kg maximum capacity (AL30C3SH10E) was used to measure the cross-flow forces.

For the side rollers, two NKL 3.230-KS frictionless tables from the company SCHNEEBERGER [22] were used. The maximum stroke of these slide tables is 0.155m, which is more than sufficient to accommodate the expected maximum oscillations. To further reduce the initial friction on the bearings (which was hindering the VIV), the slide tables were opened and the bolts were loosened. Ultimately, a friction for of approximately 0.10N on each bearing remained, which allowed VIV to occur. The friction force was estimated by matching the predicted response of a single degree of freedom system with the measured free decay of the inner frame (free-vibration layout; dry conditions) when displaced from its resting position.

A MICRO-EPSILON optic laser ILD1302-200 [23] was fixed to the upper beam in the free-vibration tests to measure the relative displacement between the inner and outer frames. The laser can record distances from 0.06m to 0.26m, whereby a maximum oscillation amplitude of 0.10m is measurable.

Both the inner and the outer frames were designed such that their natural frequencies were higher than the expected shedding frequency. After assembling the structure, and with the inner frame fixed to the outer frame (stationary layout, Figure 1c), the responses to some low intensity impacts at random locations in the inner and outer frames were measured. The following fundamental natural frequencies were observed: 13Hz for the inner frame; 8 Hz for the outer frame. The expected vortex shedding frequency at the largest flow velocity is approximately 2.5Hz.

The diameter of the cylinder is $D = 0.04$ m, and the length is $l = 0.375$ m, corresponding to the aspect ratio of 9.375. The total mass of the inner frame (accounting for the slide tables) is $m = 2.550$ kg. The corresponding mass ratio, calculated as the ratio between the mass of the structure and the mass of the displaced volume of fluid (also termed potential added mass — m_a), is $\bar{m} = m/m_a = 4m/\left(\pi l D^2 \rho_w\right) \approx 5.5$, where ρ_w is the density of water, here assumed to be 1000 kg/m^3.

For the free vibration tests (Figure 1d), two sets of springs were used. The softer set consisted of four springs, each with a stiffness of 50N/m (SODEMAAN [24], reference E05000375000M), whereas the stiffer set consisted of two springs, each with a stiffness of 170N/m (SODEMAAN, reference E05000494500S). The

measured natural frequencies of the system submerged in water, with the cylinder placed 20cm from the bottom, were 1.3 Hz for the softer springs and 1.7Hz for the stiffer springs.

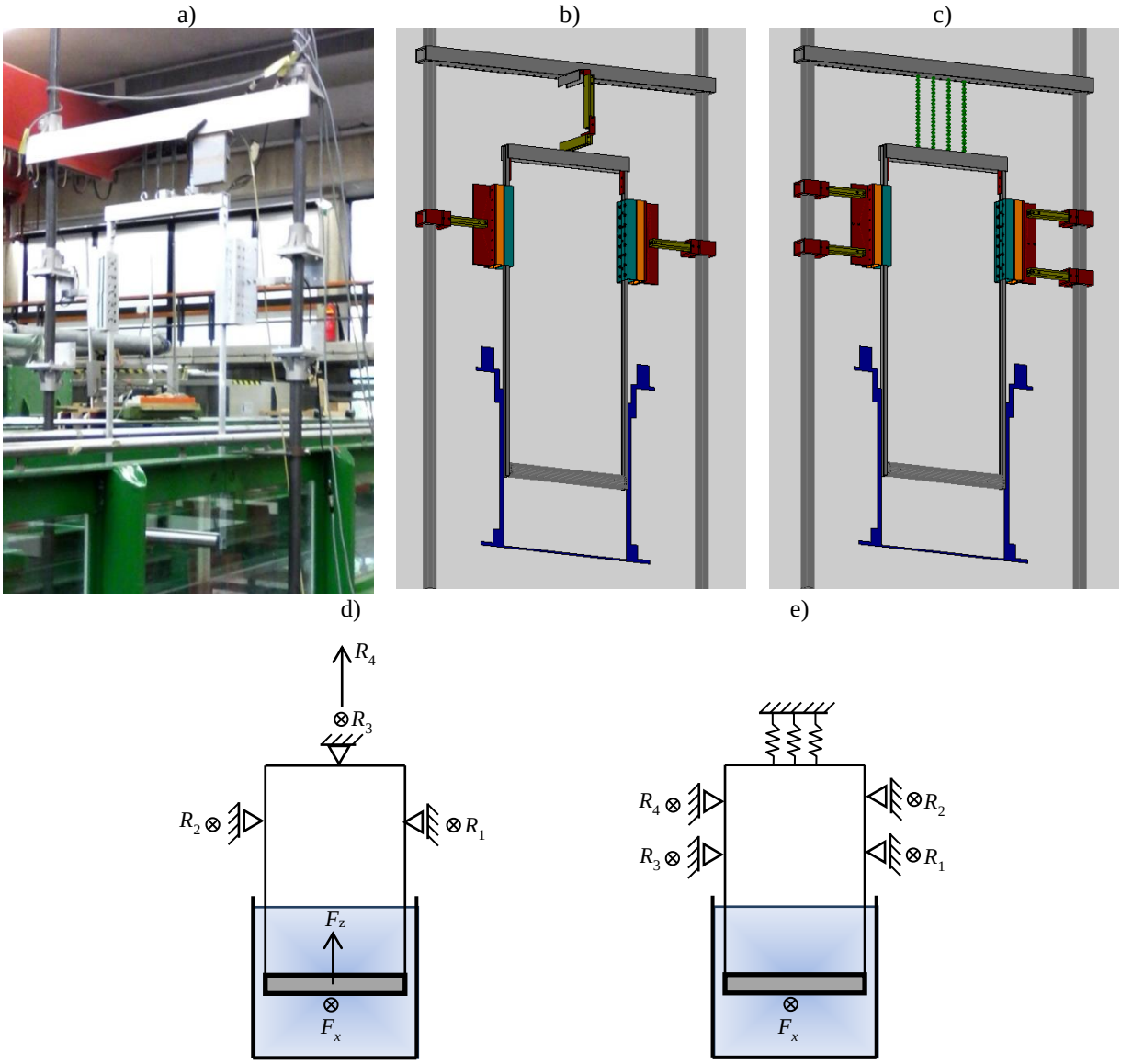

Figure 1. a) apparatus; b) schematic of stationary setup; c) schematic of free vibration setup; d) mechanical idealization of stationary experiments; e) mechanical idealization of free vibration experiments. In b) and c): grey = frames; blue = flume; yellow = load cells; green = springs; orange = bearings; red = rigid connectors

Prior to the installation of the frame, the flow profile was measured with an electromagnetic flow meter (EMS) at the longitudinal position where the structure was to be installed. The pump was turned on at discharges of Q = 40l/s and Q = 60l/s, and the fluid velocities were measured from the bottom of the flume up to the depth 0.275m, with increments of 0.025m. The time-averaged velocities V (normalized by the velocity at the top position $V_{27.5}$) are shown in Figure 2. The velocity profile resembles the logarithm profiles that are expected near boundaries. The standard deviation (in time) of the measured velocities was about 5% of $V_{27.5}$.

For the evaluation of the reduced velocity defined in eq. (2), the value $V_{27.5}$ is used for V. For each test, the value $V_{27.5}$ was measured 3m upstream of the test section.

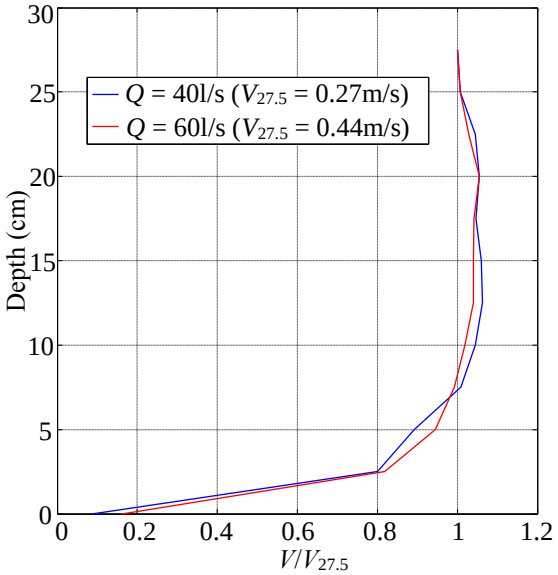

Figure 2. Velocity profile at test section

3. Stationary experiments

3.1. General procedure, measured forces and dimensionless force coefficients

The procedure for the stationary experiments is as follows: with the cylinder (frame) placed at a desired position and the fluid still, the output voltage of each load cell is shifted to zero; subsequently, the flow is started, and for each specified flow velocity, the forces are recorded by the four load cells during 3 to 4 minutes, at a sampling rate of 100Hz. Afterwards, the forces are passed through a simple low-pass filter (rectangular window removing the content above 6Hz) so that the contribution of noise and natural frequencies of the frames are removed. The tested gap G to diameter D ratios are $G/D = \{0, 0.1, 0.2, 0.3, 0.4, 0.5, 0.75, 1, 1.5, 2, 3, 4\}$, and for each gap, the discharge assumes values from 30 l/s to 60 l/s, with increments of 10 l/s. This corresponds to Reynolds numbers of 7250, 10000, 12500 and 15500).

The forces measured by the horizontal load cells (R_1, R_2, R_3) are composed of the fluid forces acting on the cylinder (F_x) and the fluid forces acting on the frame (F_{Frame}). In order to isolate the in-line forces acting on the cylinder, F_{Frame} must be removed from the total force, i.e.,

$$F_x = R_1 + R_2 + R_3 - F_{\text{Frame}} \tag{3}$$

The frame forces F_{Frame} were quantified by removing the cylinder from the frame, and subsequently placing it in water, subjecting it to the same flow velocity as the full frame, and measuring the forces. With this layout, F_{Frame} corresponds to the forces measured by the three load cells, i.e., $F_{\text{Frame}} = R_1 + R_2 + R_3$.

Note: F_{Frame} was measured only for the frame at the position corresponding to G/D=5. For the remaining positions, the forces are estimated assuming that drag is uniformly distributed along the frame, i.e.,

$$F_{\text{Frame}} = \left(2 - 0.2\frac{G}{D}\right) F_{\text{Frame}(G/D=5)} \tag{4}$$

The cross-flow force corresponds to the force measured by the vertical load cell, i.e., $F_z = R_4$.

Figure 3 depicts 50s of the time trace of the in-line (not corrected for F_{Frame}) and cross-flow forces and their frequency spectra for a discharge of 50 l/s (Re = 12500) and a gap ratio of $G/D = 4$ ($G = 0.16$ m). This example is representative of the forces measured during the stationary experiments, and is chosen to exemplify how the forces are characterized. A positive in-line force represents a force in the direction of the flow, and a positive cross-flow force represents a downward force. In this graph, forces F_{Frame} have not been subtracted.

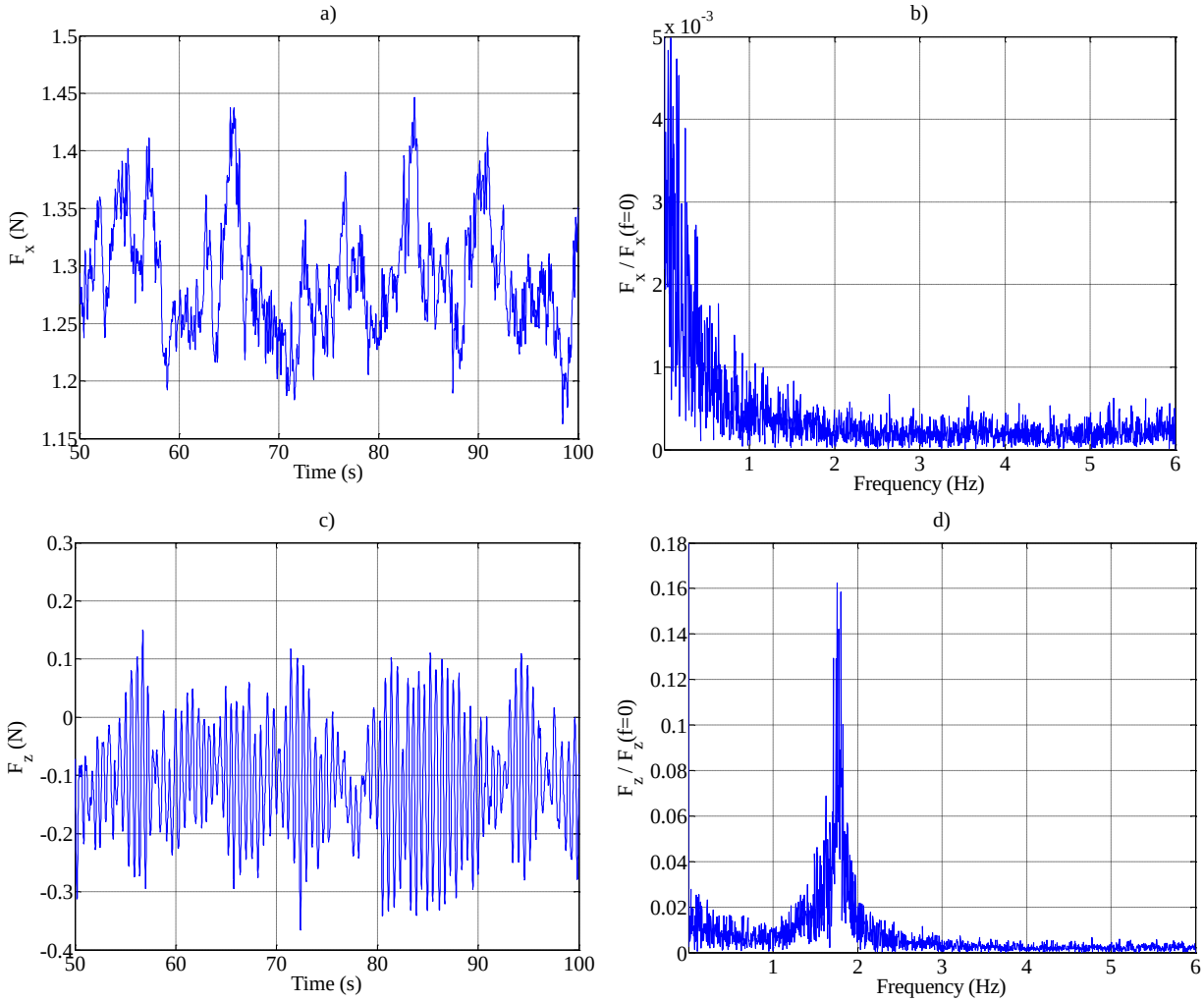

Figure 3. a) time trace of in-line force; b) frequency spectrum of in-line force; c) time trace of cross-flow forces, d) frequency spectrum of cross-flow force. $G/D = 4$.

A clear peak can be observed in the frequency spectrum of the cross-flow force. This peak corresponds to the vortex shedding frequency. According to the literature, the in-line force spectrum should contain a similar peak, though with smaller amplitude, at twice the vortex shedding frequency. Such a peak is, however, not observed in Figure 3, nor in the results reported in the remaining parts of this contribution. The reason for this is thought to be the noise, which conceals the oscillating component (literature suggests an oscillating drag coefficient around 0.0215 [2], which in this case corresponds to an oscillating force of approximately 0.02N, whereas the precision of each load cell is 0.017N). For this reason, no conclusion can be drawn regarding the oscillating part of the in-line force.

Other features observed in Figure 3 are non-zero mean values of the in-line and cross-flow forces. The mean in-line force corresponds to the drag induced by the flow. The mean cross-flow force, though of much smaller amplitude, was expected to be zero, since the cylinder is far from the boundary and thus the flow was expected to be symmetric. However, the force measured by the load cell does not correspond solely to the lift induced by the fluid: part of it corresponds to the friction at the bearings, which may act both upwards and downwards. Note that the mean cross-flow force is of the same order of magnitude as the friction in the bearings, which is 0.10 N per bearing (for the dry scenario). As will be shown later, the mean cross-flow force assumes values that exceed the friction force when the cylinder is placed closer to the bottom of the flume. In these scenarios, the mean lift is justified by the increase of the fluid pressure at the lower edge of the cylinder.

Regarding the oscillating component of the cross-flow force, even though one dominant frequency can be observed, the amplitude of oscillations is not constant in time (Figure 3c). In order to characterize the amplitude of oscillations, the root mean square (RMS) of the time trace (shifted by the mean value of each recorded signal) is used.

It is common practice to scale the fluid forces (mean values or oscillating amplitudes) by the diameter D, the length of the cylinder l, and the flow velocity V. The resulting dimensionless coefficients can thereafter be used to estimate forces on cylinders with different dimensions and/or exposed to flows with different velocities. The dimensionless force coefficients are calculated as

$$C_{x,z} = \frac{F_{x,z}}{\frac{1}{2}\rho_w l D V^2} \tag{5}$$

where ρ_w is the density of the fluid.

Similarly, the oscillating frequency of the forces (and namely of the lift force) is scaled by the flow velocity and the diameter, obtaining in this way the already mentioned Strouhal number (St), expressed as (cf. eq. (1))

$$\mathrm{St} = f_s \frac{D}{V} \tag{6}$$

In what follows, it is studied how these coefficients change with the distance to the boundary.

3.2. Gap dependency and influence of the boundary

The mean in-line coefficient C_x(mean), the mean cross-flow coefficient C_z(mean), the oscillating cross-flow coefficient C_z(osc), and the Strouhal number St are shown in Figure 4 as functions of the gap to diameter ratio G/D. Triangles represent the results obtained in the present work, solid lines correspond to the average of the coefficients over the different Reynolds numbers, and dashed and dashed-dotted lines represent results obtained by other authors.

Starting with the analysis of the mean in-line coefficients (Figure 4a), it can be observed that the force coefficient decreases slightly as the gap ratio is reduced, which is in accordance with previous works. One also observes a dependency on the Reynolds number, with the coefficient tending to decrease as the Reynolds number increases. When compared with the results obtained by Kiya and by Roshko et al. (Figure 2.21 of [25], shown in Figure 4a with a dotted line and a dash-dotted line, respectively), who considered Reynolds numbers between 10000 and 40000, one observes that the average coefficients (solid black line) obtained in the current work are slightly smaller, with the difference being around 10%. These differences may be due to the different Reynolds numbers.

Regarding the mean cross-flow coefficient (Figure 4b), its variation with the Reynolds number is the same as reported for the mean in-line coefficients, i.e., the coefficient decreases as the Reynolds number increases. Regardless of the Reynolds number, the coefficient tends to decrease as the gap ratio increases, which can be expected since the effect of the boundary becomes less pronounced as the cylinder is placed further away from it. At the gap ratios G/D = 1 and G/D = 4 the coefficients present drops which are not expected. These drops correspond, however, to forces of approximately 0.1 N, which is in the order of magnitude of the frictional forces at the bearing. As a matter of fact, for gap ratios above 0.5, the measured mean cross-flow force is always below 0.15 N, and thus the results for these positions may have been affected by the friction, and can be considered unreliable. For gap ratios below 0.5 the measured forces are larger than the friction force in the bearings, and in these cases, the average mean lift coefficient (solid black line) corresponds well with the results reported in figure 2.27 of reference [25] (represented in Figure 4b with a dotted line; a negative coefficient means that the force is directed away from the boundary).

The oscillating cross-flow coefficients and the Strouhal number (Figure 4c-d) will be analysed together. Besides the fact that both are almost not affected by the Reynolds number (at least within the range considered), the first feature to be noted is the very small force coefficient and the null Strouhal number observed for $G/D \leq 0.3$. This is justified by the suppression of vortex shedding, which was confirmed during the experiments by means of flow visualization. For bigger gap ratios, vortex shedding takes place (also confirmed via flow visualization) and the Strouhal number assumes values around 0.2 (the mean value is 0.195). Previous reports showed a small increase of the Strouhal number as the cylinder is placed closer to the bottom (10 to 15%, [17]), but such increase is not observed in this work.

In terms of the magnitude of the oscillating cross-flow coefficient, its value tends to decrease with the increase of the gap ratio, stabilizing at the value of 0.1. The values herein obtained are considerably smaller than the ones presented by Lei et al. [16], represented with a dotted line in Figure 4c. The reason for the difference

may be attributed to the friction at the bearing and to the experimental conditions (Lei et al. performed experiments in a wind tunnel).

The results presented here showed that the setup is capable of reproducing the main features of VIV of stationary cylinders, namely the suppression of vortex shedding for $G/D \leq 0.3$ and the mean cross-flow force that tends to vanish as the gap ratio increases. Also the vortex shedding frequency and the magnitude of the in-line forces show a good correspondence. On the contrary, the amplitude of the oscillating cross-flow force did not show a good correspondence with previous works. The reason for the latter is attributed to different test conditions and to friction at the bearings. In any case, the cross-flow force on stationary cylinder is of insignificant relevance for the main purpose of this work, which is addressed in the following sections.

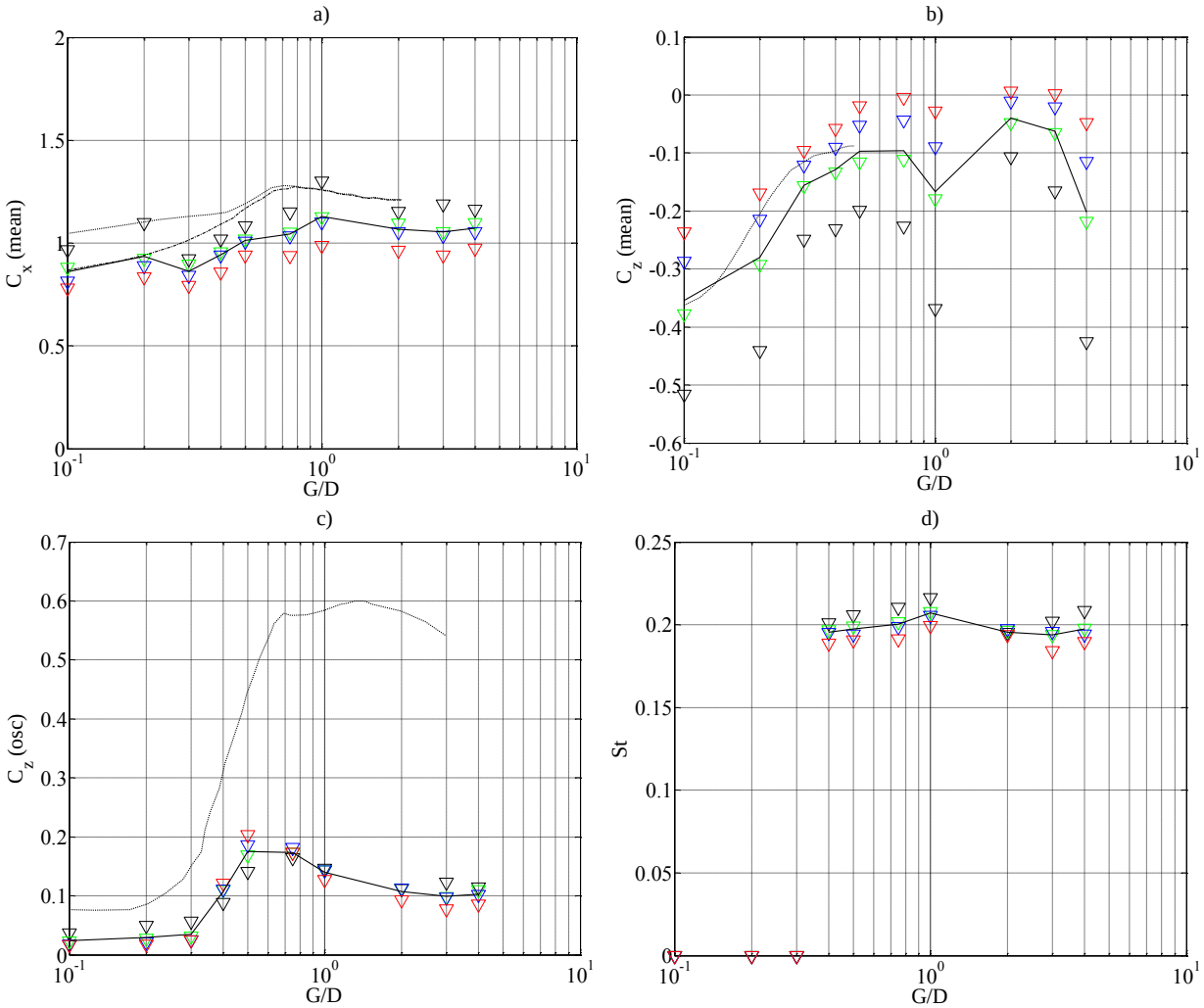

Figure 4. a) mean in-line force coefficient (Solid line = average; dotted line = Kiya [25]; dash-dotted line Roshko et al. [25]); b) mean cross-flow force coefficient (Solid line = average; dotted line = reference [25]); c) oscillating (RMS) cross-flow force coefficient (Solid line = average; dotted line = Lei et. al [16]); d) Strouhal number (Solid line = average). Re = 7250 (black), 10000 (green), 12500 (blue) and 15500 (red). (For interpretation of the references to colour in this figure legend, the reader is referred to the web version of this article.)

4. Free vibration experiments

4.1. General procedure and measured deflections and forces

With the flume filled with still water, the cylinder is placed at a desired position and the output voltages of the load cells and of the laser are set to zero. With the cylinder at rest, the flow is started at the discharge of 25l/s, and then increased slowly up to the maximum discharge 80l/s (Re = 6500 to 20000). For each small discharge

increment, the forces on the four AL10 load cells and the displacements given by the optic laser are recorded for at least 3 minutes, at a sampling frequency of 100Hz. The total in-line force corresponds to the summation of the forces measured by the four load cells minus the force on the frame, as in eq. (3).

The tested gap to diameter ratios are $G/D = \{0, 0.25, 0.5, 0.75, 1, 1.5, 2, 3, 4, 5\}$. The gap ratios are divided into three groups, according to the response of the cylinder: a group comprising the large gaps, such that the influence of the boundary is very small; a group in which the boundary influences the response of the cylinder, but no contact between the cylinder and the bottom occurs; and a group comprising the small gap ratios, where the cylinder touches the bottom of the flume when excited by the flow.

Figure 5 shows two time traces of the displacements (divided by the diameter, u_z/D) and the in-line forces (by means of the force coefficient C_x) when the reduced flow velocity, as defined in eq. (2), is $V_r = 6.3$ and $V_r = 12$ (the gap ratio is $G/D = 4$, and the soft spring set is used). These time traces are representative of the response of the cylinder inside and outside the lock-in region, respectively. The in-line forces are not corrected for F_{Frame}.

For the reduced flow velocity $V_r = 6.3$, the deflections of the cylinder (Figure 5a) show a clear harmonic behaviour with an amplitude of one diameter. In turn, the in-line forces (Figure 5c) also show a considerable dynamic component, but with less constant amplitude in time (the dominant frequency of the in-line force is twice the dominant frequency of the displacements). These two time traces are typical for the lock-in regime, where (as seen later) the maximum deflections reach values between $1D$ (at the beginning of lock-in) and $0.6D$ (at the end).

At the reduced flow velocity $V_r = 12$, the deflections of the cylinder are very small (Figure 5b), and so are the oscillations of the in-line force (Figure 5d). No clear oscillation frequency can be discerned from the time traces. These time traces are typical outside of the lock-in region, where very small oscillations are expected.

To characterize the displacements of the cylinder, in this work the amplitude of oscillation A (taken as the average of all local maxima through the time series) and the corresponding frequency f_{cyl} (taken as the dominant frequency observed in the frequency spectra of the displacements) are used. The in-line force is characterized based on the expression

$$F_x(t) \approx \bar{F}_x + F_{x1} \sin\left(2\pi f_{\text{Cyl}} t + \phi_1\right) + F_{x2} \sin\left(4\pi f_{\text{Cyl}} t + \phi_2\right) \tag{7}$$

where $\bar{F}_x$ is the mean value, F_{x1} and F_{x2} are the variation amplitudes associated with frequencies f_{cyl} and $2 f_{\text{cyl}}$, respectively, and ϕ_1 and ϕ_2 are phase angles associated with the same frequencies.

Because outside of the lock-in regime the oscillation of the cylinder do not show regular patterns, the amplitudes F_{x1} and F_{x2} and the phases ϕ_1 and ϕ_2 are calculated only for the cases in which the vertical oscillation of the cylinder is above $0.1D$. These values are found by minimizing the errors (with the least square procedure) between the measured forces and the forces returned by eq. (7) for each vertical cycle of the cylinder, and subsequently averaging the set of values obtained for all complete cycles available in the time record. The values $\bar{F}_x$, F_{x1} and F_{x2} can be normalized according to eq. (5), thus obtaining the in-line force coefficients $\bar{C}_x$, C_{x1} and C_{x2}.

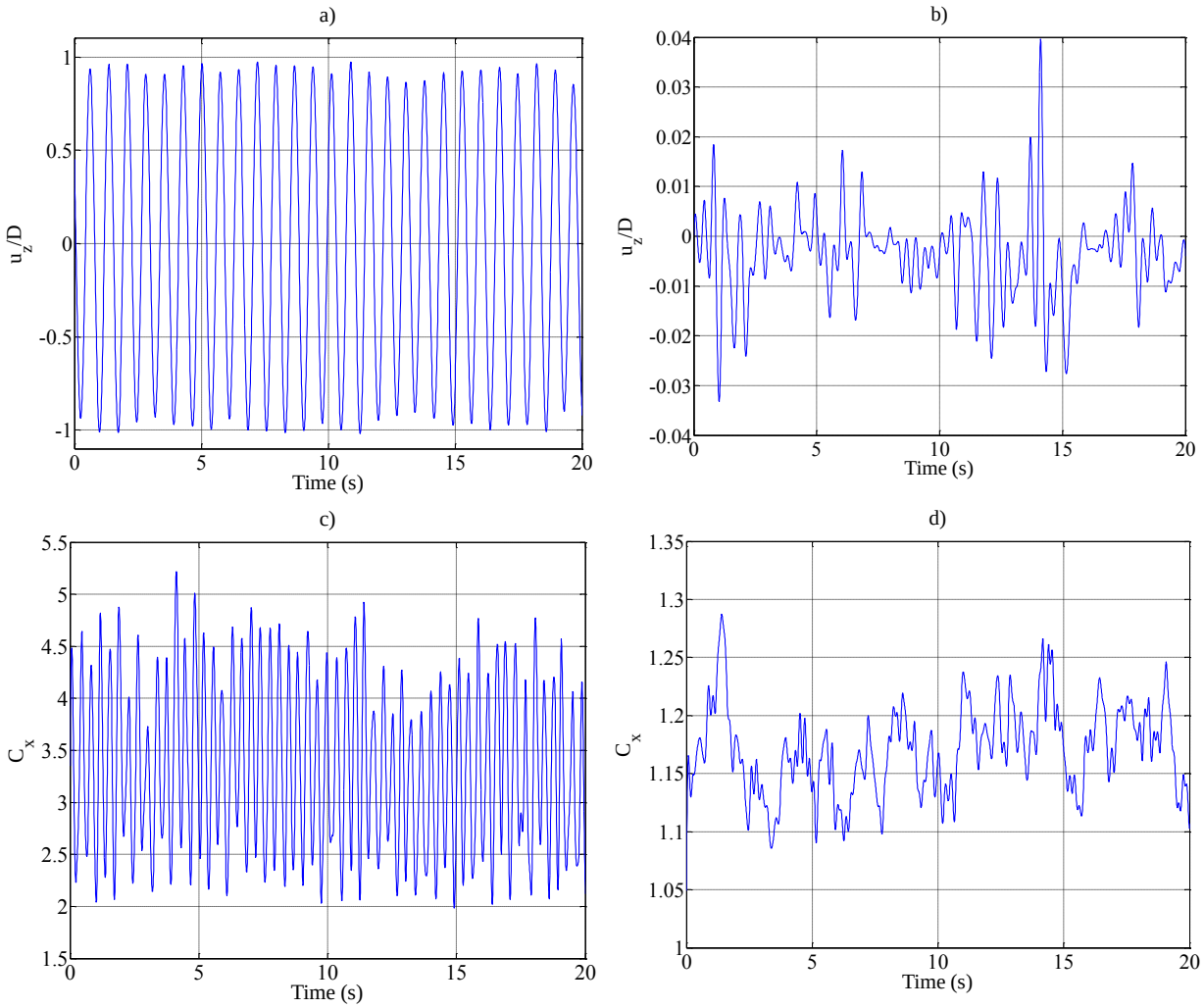

Figure 5. Time traces of normalized vertical displacements (u_z/D) for V_r = 6.3 (a) and V_r = 12 (b), and of in-line force coefficients (C_x) for V_r = 6.3 (c) and V_r = 12 (d). G/D = 4. Soft spring set

4.2. Large gap ratios

The gap ratios $G/D = \{2,3,4,5\}$ are included in this group. Figure 6 shows the obtained oscillation amplitude A and oscillation frequency f_{Cyl} as functions of the reduced flow velocity V_r. The obtained values are accompanied by the results of Blevins et al. [10] (mass ratio = 6.4; damping = 2%).

Analysing the amplitudes of oscillations (Figure 6a), it can be observed that there is a range of flow velocities where the oscillations are negligible ($V_r < 4$), then a narrow interval where there is a sudden increase of the amplitude of oscillations (initial branch, $4 < V_r < 5$), a zone where the oscillations are in the order of one diameter (upper branch, $5 < V_r < 7$), a zone where the oscillations tend to decrease but are still greater than 0.5 D (lower branch, $7 < V_r < 9$) and, finally, a sudden drop of the oscillation amplitude and a region where the oscillations are again negligible ($V_r > 9$). These features are also present in the results obtained by Blevins et al. [10], but in their case the lock-in region is slight narrower, the amplitudes of oscillations are a bit lower, and the drop of the amplitude is less sharp. These differences are due to the different test conditions. While in Blevins et al. the damping is viscous (2% of the critical) and the mass ratio is 6.4, in the current experiments the damping source is frictional and the mass ratio is 5.5. In their report, Blevins et al. also present the results for different damping values and different mass ratios, and conclude that by decreasing the damping the amplitude of oscillations increases and that by decreasing the mass ratio the lock-in region widens. These conclusions are consistent with the differences verified between this report and reference [10].

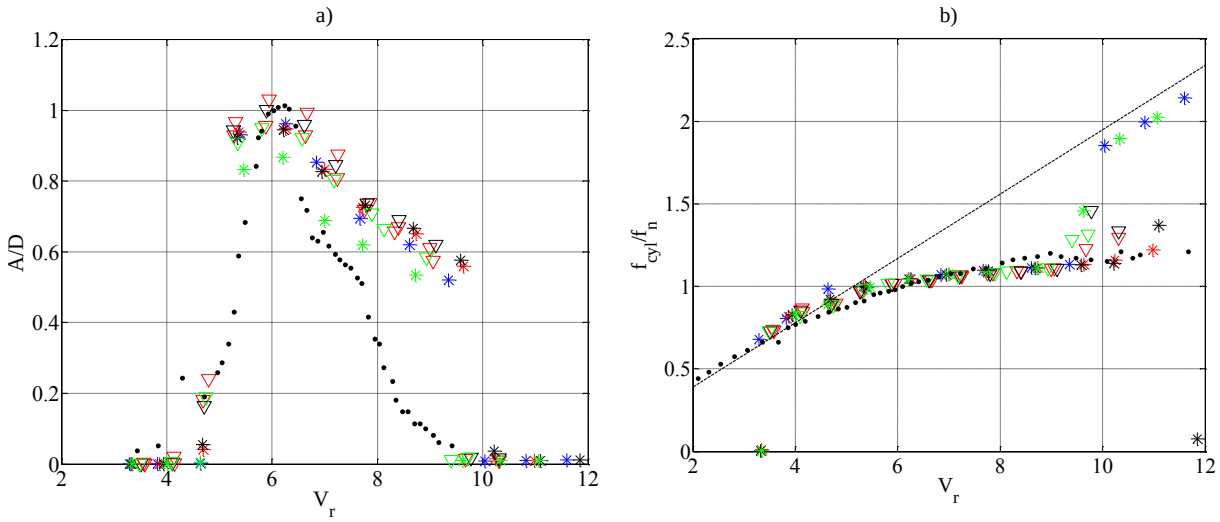

Figure 6. a) amplitude of oscillations; b) frequency of oscillations. Gap ratio (G/D) = 5 (blue), 4 (red), 3 (black), and 2 (green). Stars = soft springs; triangles = stiff springs; black dots = Blevins et al. [10]; black dashed line = Strouhal frequency (St = 0.195) . (For interpretation of the references to colour in this figure legend, the reader is referred to the web version of this article.)

Regarding the oscillation frequency f_{cyl}, the observed values follow very closely the results reported in [10]. Inside the lock-in region ($5 < V_r < 9$) the oscillation frequency is close to the natural frequency f_n of the immersed cylinder (1.3 Hz for the soft spring set and 1.7 Hz for the stiff spring set), which is also in accordance with the conclusions of previous works. Outside of the lock-in region, the frequency f_{cyl} tends to follow the Strouhal frequency, which in Figure 6b is denoted with a black dotted line (St = 0.195).

Figure 7 shows the in-line coefficients $\bar{C}_x$, C_{x1} and C_{x2}, and the phase angles ϕ_1 and ϕ_2 as functions of the reduced velocity V_r for the four gap ratios considered in this group. The mean in-line coefficients are accompanied by the results reported in reference [10]. Both the mean (Figure 7a) and the oscillating (Figures 7b,d) coefficients assume the maximum value at the reduced velocity $V_r = 5$, which also corresponds to the onset of the lock-in region. The coefficients then become smaller with the increase of the flow velocity, reaching their minimum at the end of the lock-in region. Outside of the lock-in region the oscillating coefficients and corresponding phases are not shown because in these cases the oscillations of the cylinder are very small (under 0.1*D*) and, as observed in Figure 5d, the forces do not show a regular harmonic time trace. The mean coefficient stabilizes between 1.0 and 1.2, which is in correspondence with the in-line coefficient for stationary cylinders. The evolution of the mean in-line coefficient $\bar{C}_x$ is in accordance with the results presented in reference [10], but its values are slightly larger and the amplification region is a bit wider. Like for the oscillations, these differences can be justified by the different damping mechanisms and different mass ratios. The evolution of the oscillating components C_{x1} and C_{x2} is also in accordance with the results presented by Khalak and Williamson [6], who compared the maximum in-line force coefficient and the corresponding mean value and show that the difference between these two values presents a peak around $V_r = 5$ and decreases to almost zero as the flow velocity is increased (Figure 3 of reference [6]).

By comparing the amplitudes of the oscillating in-line coefficients, one observes that the coefficient C_{x2} is about four times bigger than the coefficient C_{x1}, which supports the conclusion that the dominant frequency is indeed twice the oscillating frequency of the cylinder.

As for the phase angles, no clear tendency seem to exist in the behaviour of ϕ_1 (the phase angle has a large scatter). The phase angle ϕ_2, on the contrary, reveals a clear trend inside the lock-in region. It starts with the value of $\pi/3$, and then increases to approximately $2\pi/3$.

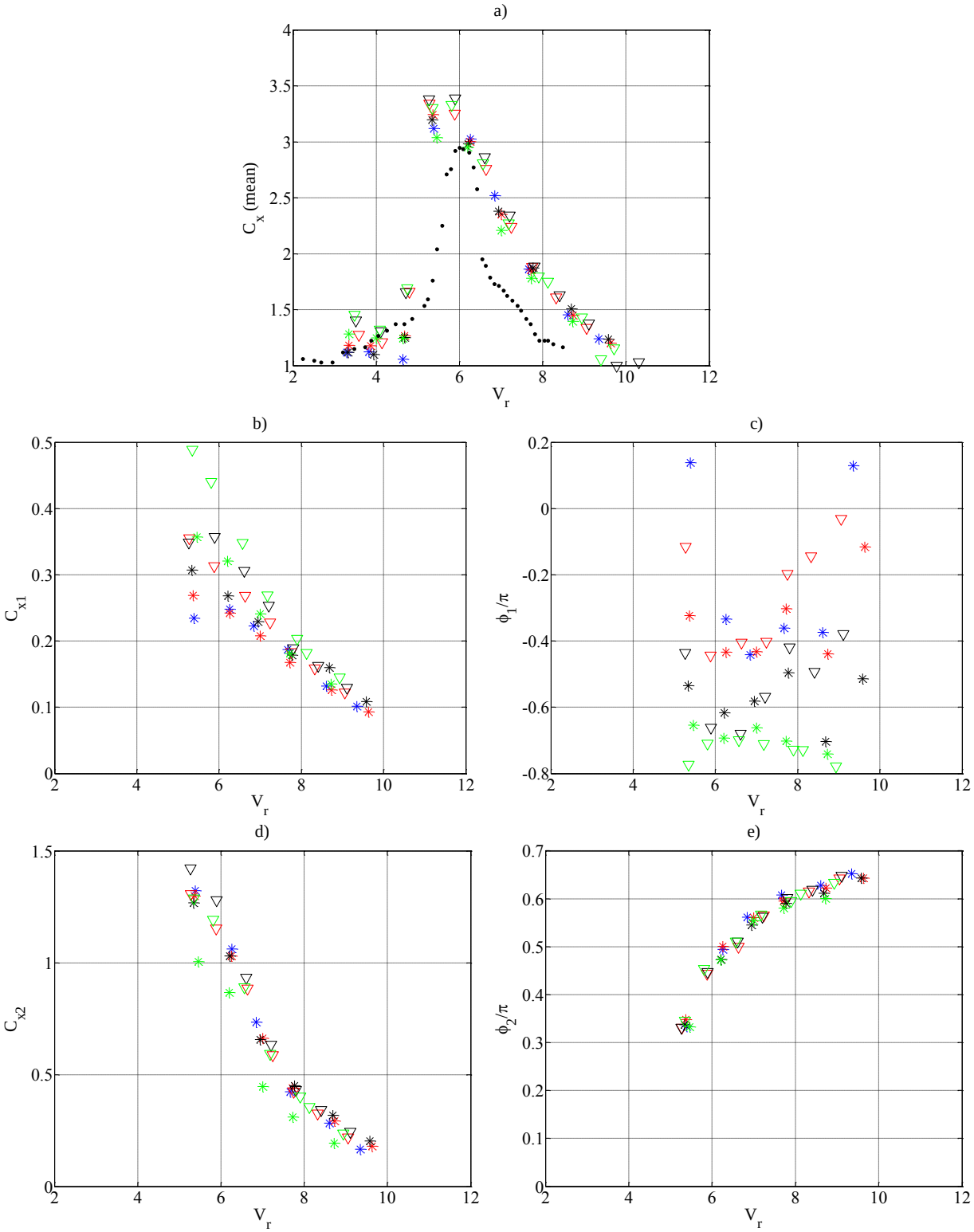

Figure 7. a) mean in-line force coefficient; b) oscillating in-line force coefficient with frequency f_{cyl}; c) Phase ϕ_1; d) oscillating in-line force coefficient with frequency $2f_{cyl}$; e) Phase ϕ_2. Gap ratio (G/D) = 5 (blue), 4 (red), 3 (black), and 2 (green). Stars = soft springs; triangles = stiff springs; black dots = Blevins et al. [10]. (For interpretation of the references to colour in this figure legend, the reader is referred to the web version of this article.)

Most of the empirical models based on free vibrations are constructed with the purpose of matching the measured vertical motion of the cylinder [11]. These models can be improved if, in addition to the vertical motion, the in-line force is also matched, in terms of its mean value, oscillation amplitude, and phase angle with respect to the vertical oscillations. In that sense, the information provided in this work can be useful, since a

clear dependence of the amplitude and phase of the in-line force on the reduced velocity has been observed. To the best of the authors' knowledge, no previous work has shown such a dependence. The improvement associated with matching the in-line force may allow for more accurate predictions of the response of cylindrical structures that are not constrained in the in-line direction.

In general, there is a very good correspondence of the results associated with different gap ratios, showing that for gaps greater than two diameters the bottom does not have significant influence on the response of the cylinder, and that the stiffness of the spring also does not play a significant role. There is however a small scatter of the mean in-line force for reduced velocities smaller than 5 (before the lock-in region).

4.3. Medium gap ratios

This group includes the gap ratios of $G/D = \{1.5, 1, 0.75\}$. During the experiments no impact with the bottom was registered, and the motion of the cylinder revealed to be symmetric with respect to the equilibrium position, i.e., the upward and downward deflections showed roughly the same value (the downward motion was not smaller than 90% of the upward motion). Figure 8 depicts the maximum amplitudes and frequencies of oscillation as functions of the reduced velocity, while Figure 9 shows the in-line force coefficients and phase angles also as functions of the reduced velocity.

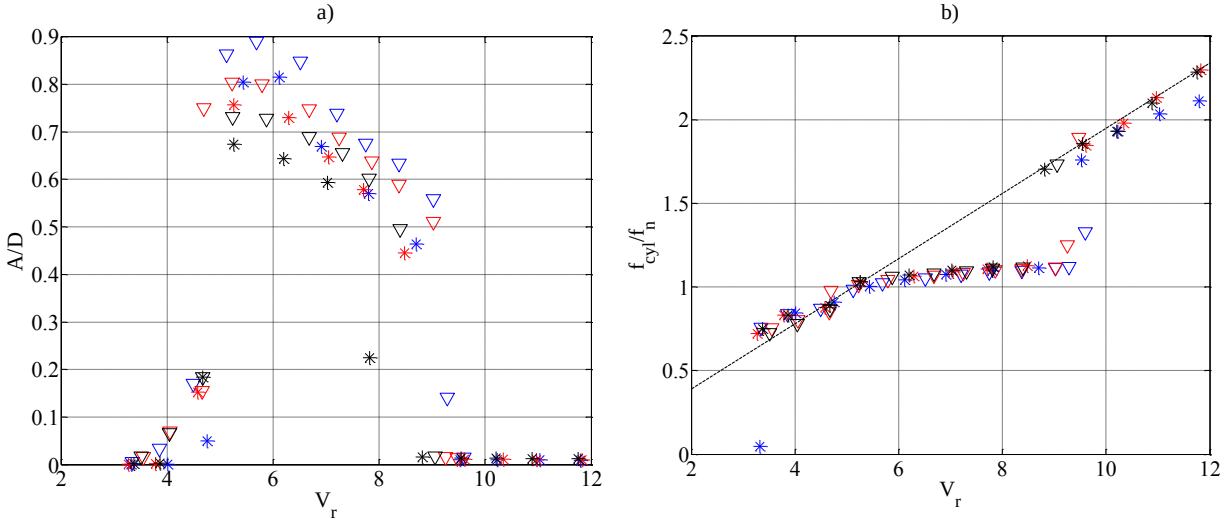

Figure 8. a) amplitude of oscillations; b) frequency of oscillations. Gap ratio (G/D) = 1.5 (blue), 1.0 (red), and 0.75 (black). Stars = soft springs; triangles = stiff springs; black dashed line = Strouhal frequency (St = 0.195). (For interpretation of the references to colour in this figure legend, the reader is referred to the web version of this article.)

It is evident from Figure 8a that as the cylinder is placed closer to the bottom, the maximum amplitude of oscillation decreases. The explanation for this decrease can be found in the vertical force that acts on cylinders near a plane boundary (an upward force has been registered in the stationary experiments, suggesting the existence of a similar force when a freely vibrating cylinder approaches the boundary). The upward directed vertical force opposes the downward motion of the cylinder, thus extracting energy from the cylinder and reducing the amplitude of vibrations. By lowering the equilibrium position of the cylinder, the force is activated earlier, resulting in a more pronounced attenuation of the oscillations.

The stiffness of the springs (or similarly, the Reynolds number) also plays a role in the response of the cylinder, with the deflections being about 10% larger when the stiff springs are used (the triangles tend to be above the corresponding stars; for the same reduced velocity, the Reynolds number for the stiff springs is about 30% higher than for the soft springs). The oscillation frequencies follow the same trend as in the case of the previous group, being close to the natural frequency of the cylinder during lock-in and close to the Strouhal frequency (demarked with black dotted line in Figure 8b) outside of this region.

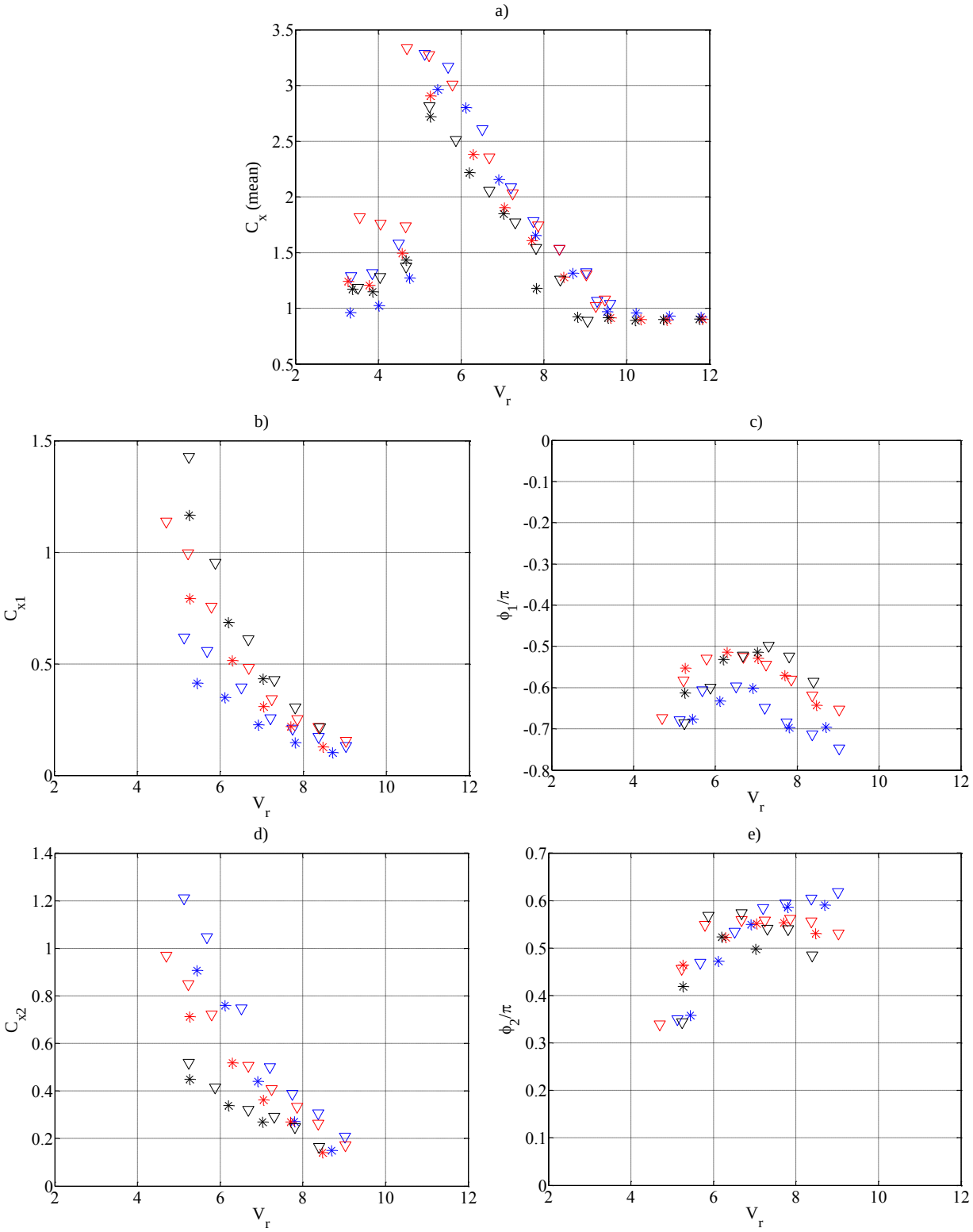

Figure 9. a) mean in-line force coefficient; b) oscillating in-line force coefficient with frequency f_{Cyl}; c) Phase ϕ_1; d) oscillating in-line force coefficient with frequency $2f_{Cyl}$; e) Phase ϕ_2. Gap ratio (G/D) = 1.5 (blue), 1.0 (red), and 0.75 (black). (For interpretation of the references to colour in this figure legend, the reader is referred to the web version of this article.)

Regarding the in-line forces induced by the flow, and starting by analysing the mean component, it can be concluded that during lock-in the mean in-line force slightly decreases as the gap ratio is made smaller (Figure 9a). Outside the lock-in region, no significant differences in the mean force are observed for the different gap ratios. Note that before the lock-in region (V_r < 5) the in-line coefficients are bigger than after the region (V_r > 9),

which is consistent with the reduction of the coefficient with increasing Reynolds number, as reported in Figure 5a.

Concerning the oscillating components of the in-line force, the component C_{x1} increases with a decreasing gap ratio, while the component C_{x2} follows the opposite trend. Interestingly, the sum of the amplitudes C_{x1} and C_{x2} yields the same resultant for the three gap ratios, which is also the same as the value obtained for the gaps considered in the previous group. The reason for the increase of C_{x1} and the decrease of C_{x2} is, presumably, the stronger vortices being shed from the upper part of the cylinder when compared to those being shed from the lower part. This difference in strength of the vortices is caused by the presence of the boundary, which interrupts the vortex formation (recall that for the stationary cylinder, when the gap ratio is smaller than 0.3, vortices are suppressed).

The phase angle ϕ_1 lies between $-2\pi/3$ and $-\pi/2$, while the phase angle ϕ_2 lies between $\pi/3$ and $2\pi/3$.

4.4. Small gap ratios

In this group, the gap ratios of $G/D = \{0.5, 0.25, 0\}$ are included (for the gap ratio 0, the cylinder is almost touching the boundary). For these three positions, the cylinder touched the bottom repeatedly during the experiments, and its motion was consequently not symmetric. Figure 10 illustrates five seconds of the time traces of the displacement of the cylinder and of the in-line forces (by means of the corresponding force coefficients), for the gap ratio $G/D = 0.25$ and reduced velocity $V_r = 7.8$, using the softer spring set. Both plots depict unfiltered results.

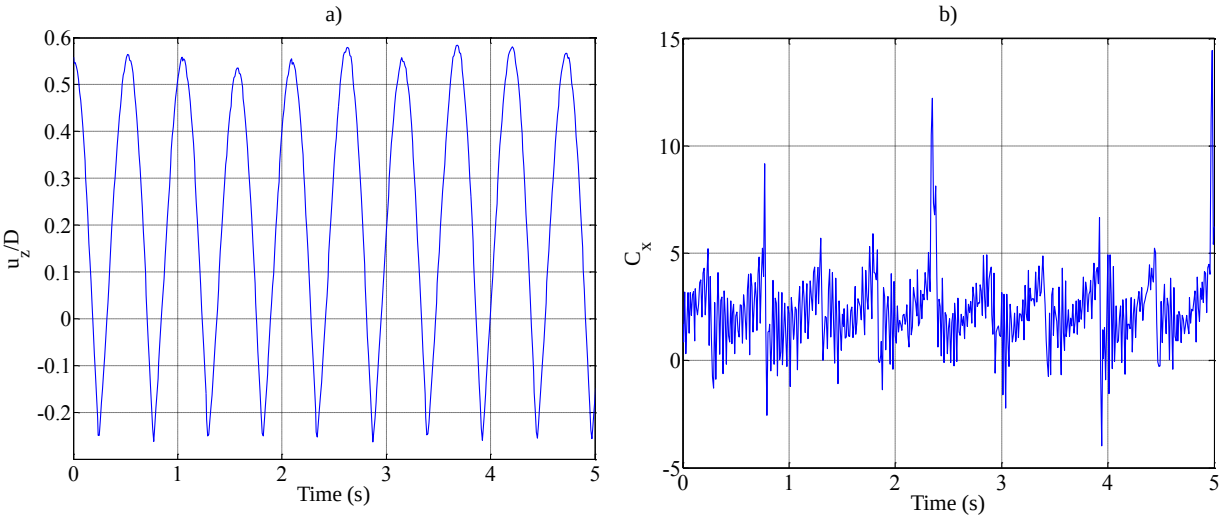

Figure 10. Time traces of: a) vertical displacements (u_z); b) In-line force. V_r = 7.8. G/D = 0.25. Soft springs set.

The impact of the cylinder against the bottom of the flume is very clear in the left plot: note the discontinuity of the velocities every time that the cylinder reaches its lowest position. The highest upward deflection is quite constant over time, and well exceeds the downward deflection.

Concerning the in-line force, a peak can be distinguished every time an impact occurs (in some cases, the force reaches 7 times its mean value). These in-line peaks are associated with the reaction of the flume on the cylinder, which is not purely vertical. Furthermore, the force signal shows a high frequency content, which is a consequence of the structural vibrations originated by the impact. After being passed through the low-pass filter, the in-line force still revealed a peak every time that an impact occurred. For this reason, the in-line forces are considered unreliable (in the sense that they are not induced by the flow) and therefore will not be analysed for these small gap ratios.

The maximum upward deflection (A^+) and the dominant frequency of the motion of the cylinder are depicted in Figure 11 as functions of the reduced velocity.

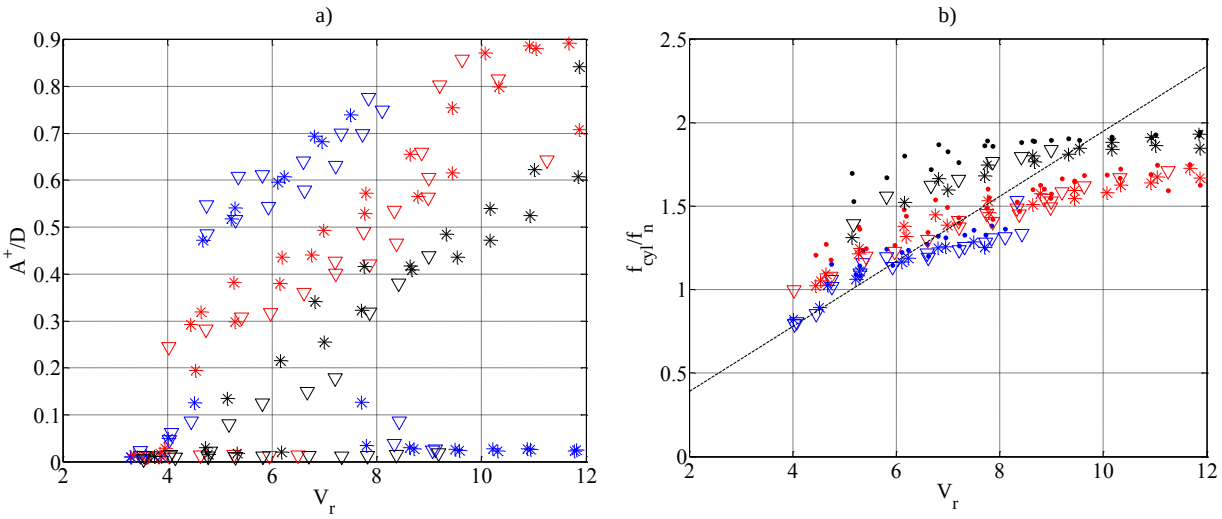

Figure 11. a) upward deflection; b) frequency of oscillations. Gap ratio = 0.5 (blue), 0.25 (red), and 0 (black). Stars = soft springs; triangles = stiff springs; dots = eq. (8); black dashed line = Strouhal frequency (St = 0.195). (For interpretation of the references to colour in this figure legend, the reader is referred to the web version of this article.)

In contrast to the previous scenarios in which the amplitude of oscillation was found to reach a maximum around the reduced velocity of $V_r = 6$, the deflection increases with increasing flow velocity in the case of small gap ratios. Also, the frequency of oscillation increases linearly with the flow velocity, and it does not follow the natural frequency of the structure nor the Strouhal frequency. Instead, the oscillation frequency follows approximately the expression

$$f_{\text{cyl}} = \frac{\pi f_n}{\cos^{-1}\left(-G/A^+\right)} \tag{8}$$

which corresponds to the natural frequency of the spring-mass system that is displaced upwards by A^+ (as in Figure 11a) and whose downwards displacement cannot exceed G (the gap) due to a rigid constraint, assuming that the impact is perfectly elastic. These frequencies, as estimated through eq. (8), are represented in Figure 11b by means of dots (for the calculation of the frequencies for the case in which the cylinder is touching the bottom, a very small gap G = 0.0015 m was assumed).

The increase of the frequency was evident during the experiments, since the impact noise was heard at higher frequencies every time the flow velocity was increased.

For the gap ratio of $G/D = 0.5$, the oscillations die out above the reduced velocity $V_r = 8$. For the remaining gap ratios, and within the tested reduced velocities, the deflection keeps on increasing, reaching a maximum amplitude of $A^+ = 0.9D$, which is comparable to the amplitudes of oscillation when the cylinder is sufficiently far from the boundary.

The results presented in this work are not in accordance with the results presented by Fredsoe et al (Figure 11a from [19]). In their work, there is a gap-dependent reduced velocity above which the amplitude of the deflections starts to decrease slowly (e.g., $V_r = 6$ for $G/D = 0.5$ and $V_r = 8$ for $G/D = 0.14$), which is not observed in our experiments. Also, the maximum deflections reported in [19] are considerably larger than the ones depicted in Figures 11a (in Fredsoe et al, the maximum deflections are between $1D$ and $1.6D$, while we observed a maximum deflection of less than $0.9D$). The reason for the different behaviour may be the different test conditions, namely the mass ratio, since in [19] the mass ratio is 1 while in this work it is 5.5.

4.5. Relevance of observed results for the analysis of tubular structures on the seabed

In the previous sections it is concluded that the bottom has no influence on the response of a cylinder placed two diameters (or more) above that boundary. It is also observed that for smaller gaps, and as long as the cylinder does not hit the bottom, the amplitude of oscillations tend to decrease with the boundary proximity. However, when the equilibrium position of the cylinder is too close to the boundary (or even touching it), the

impact at the bottom will change considerably the behaviour of the fluid-structure system, widening the range of flow velocities for which amplifications are observed, and making oscillations stronger in terms of amplitude and frequency as the flow velocity is increased. Note that this feature could not be inferred from the stationary experiments, in which suppression of vortex shedding was observed when the gap was too small (below one third of the diameter).

For cylindrical structures lying on the seabed (such as pipelines or power cables), the mentioned observations suggest that neglecting the proximity of the boundary is not necessarily conservative. On one side, it is a fact that when the boundary is not considered, lower flow velocities are needed for the pipeline/cable to oscillate with considerable amplitudes. However, on the other hand, when higher flow velocities are reached the pipeline/cable will oscillate not only with considerable amplitude, but also at a higher frequency, which may result in the reduction of its operational lifetime due to fatigue. Additionally, the impact of the structure on the ground may generate waves that propagate towards its extremities, eventually pulling them out of the ground and increasing the length of the exposed span.

5. Numerical model for VIV of a cylinder positioned near a plane boundary

The results described in the previous two sections can be used to construct empirical models that predict quantitatively the response of rigid cylindrical structures subjected to flows. These models can be further extended to predict the response of flexible structures, assuming for that matter that fluid forces on a given section do not depend on the response of neighbouring sections.

One popular type of empirical models is the wake oscillator. In this model, a "wake variable" that represents the fluid force is described through a non-linear differential equation, which has the forcing term (right hand side) dependent on the motion of the cylinder. There are several options for the exact form of the non-linear equation to be used, being the Van der Pol equation chosen in this work [11,12]. In what follows, the wake oscillator model is briefly described and then adapted to account for the findings of the free vibration experiments in the proximity of a boundary.

5.1. Wake oscillator model

Consider a cylindrical body, with diameter D and mass per unit length m, that is connected vertically to a fixed surface through distributed springs k_z and distributed dampers c_z, and horizontally through springs k_x and dampers c_x (Figure 12a). The cylinder is exposed to flow with velocity V and angle of attack α, thus being subjected to time dependent horizontal F_x and vertical F_z fluid forces (per unit length), which cause the mass to respond dynamically with time varying horizontal u_x and vertical u_z displacements.

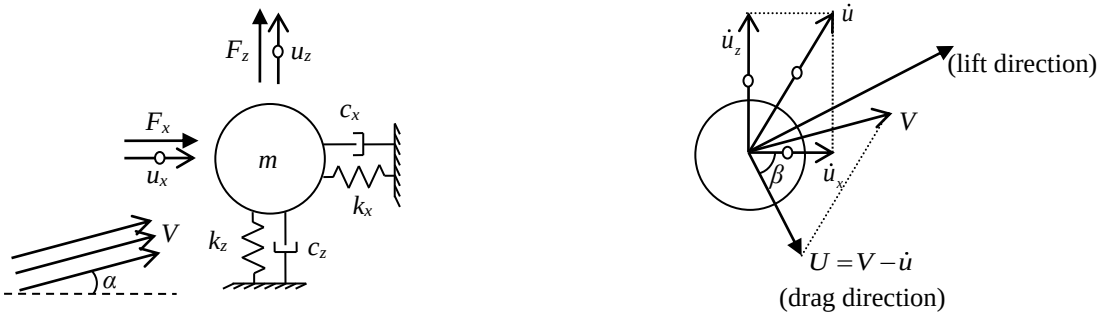

Figure 12. a) model of a cylindrical mass exposed to a flow; b) drag and lift directions

The equations of motion of the cylinder are (overdots represent time derivatives)

$$\begin{aligned} m\ddot{u}_x + c_x\dot{u}_x + k_x u_x &= F_x \\ m\ddot{u}_z + c_z\dot{u}_z + k_z u_z &= F_z \end{aligned} \tag{9}$$

For convenience, the fluid forces are split into two distinct parts, one that corresponds to the inertia force of the displaced fluid ($F_x^{(1)} = -m_a\ddot{u}_x$ and $F_z^{(1)} = -m_a\ddot{u}_z$, with $m_a = \frac{\pi}{4}D^2\rho_w$ being the ideal added mass), and a second part that corresponds to the rest ($F_x^{(2)}$ and $F_z^{(2)}$). In this way, the equations of motion can be rewritten as

$$\begin{aligned}\left(m+m_a\right)\ddot{u}_x + c_x\dot{u}_x + k_x u_x &= F_x^{(2)} \\ \left(m+m_a\right)\ddot{u}_z + c_z\dot{u}_z + k_z u_z &= F_z^{(2)}\end{aligned} \tag{10}$$

Regarding the forces $F_x^{(2)}$ and $F_z^{(2)}$, these can be decomposed into a drag component F_D in line with the instantaneous flow direction, and a lift component F_L perpendicular to the instantaneous flow (see Figure 12b for the direction of the drag and lift forces and for angle β):

$$\begin{aligned}F_x^{(2)} &= F_D\cos\beta - F_L\sin\beta \\ F_z^2 &= F_D\sin\beta + F_L\cos\beta \\ \cos\beta &= \frac{V\cos\alpha - \dot{u}_x}{U} \\ \sin\beta &= \frac{V\sin\alpha - \dot{u}_z}{U} \\ U &= \sqrt{\left(V\cos\alpha - \dot{u}_x\right)^2 + \left(V\sin\alpha - \dot{u}_z\right)^2}\end{aligned} \tag{11}$$

The drag force is assumed to be proportional to the square of the relative velocity U according to

$$F_D = \frac{1}{2}\rho_w D\, C_{D0}\, U^2 \tag{12}$$

where C_{D0} is a drag coefficient (a possible option is the mean in-line force coefficient obtained in stationary experiments). The lift force is defined in a similar manner, but its amplitude is also dependent on a wake variable q that simulates the self-exciting behaviour of the vortex street:

$$F_L = \frac{q}{4}\rho_w D\, C_{L0}\, U^2 \tag{13}$$

The lift coefficient C_{L0} is usually assumed to be the oscillating cross-flow coefficient obtained from the stationary experiments. The time dependent wake variable q is described by the van der Pol equation

$$\ddot{q} + \varepsilon\,\omega_{\mathrm{St}}\left(q^2-1\right)\dot{q} + \omega_{\mathrm{St}}^2\, q = \frac{A}{D}\left(\ddot{u}_z\cos\alpha - \ddot{u}_x\sin\alpha\right) \tag{14}$$

where ε and A are tuning parameters (tuned such that, for a wide range of flow velocities, the maximum amplitudes of displacements fit the amplitudes obtained in the free vibration tests), and ω_{St} is the radial Strouhal frequency ($2\pi f_{\mathrm{St}}$, see equation (1)). The forcing term for the wake variable is the acceleration in the cross-flow direction, as suggested by Facchinetti et al. [11].

Putting equations (10)-(14) together results in the following system of non-linear differential equations

$$\begin{cases}\left(m+m_a\right)\ddot{u}_x + c_x\dot{u}_x + k_x u_x = \dfrac{1}{2}\rho_w D\left[C_{D0}\left(V\cos\alpha - \dot{u}_x\right) - \dfrac{q}{2}C_{L0}\left(V\sin\alpha - \dot{u}_z\right)\right]U \\ \left(m+m_a\right)\ddot{u}_z + c_z\dot{u}_z + k_z u_z = \dfrac{1}{2}\rho_w D\left[C_{D0}\left(V\sin\alpha - \dot{u}_z\right) + \dfrac{q}{2}C_{L0}\left(V\cos\alpha - \dot{u}_x\right)\right]U \\ \ddot{q} + \varepsilon\,\omega_{\mathrm{St}}\left(q^2-1\right)\dot{q} + \omega_{\mathrm{St}}^2\, q = \dfrac{A}{D}\left(\ddot{u}_z\cos\alpha - \ddot{u}_x\sin\alpha\right)\end{cases} \tag{15}$$

which can be solved for u_x, u_z and q using a fourth order Runge-Kutta method.

In what follows, the system of equations (15) is used to replicate the cross-flow displacements that were observed during the free vibration experiments. For that, the displacements u_x are set to zero, and the following values are assumed: m = 6.75 kg/m; m_a = 1.25 kg/m; k_z = 535 N/m^2; c_z = 2.4 N.s/m^2 (2% of critical damping); D = 0.04 m; ρ_w = 1000 kg/m^3; C_{D0} = 1.2; C_{L0} = 0.3; α = 0; St = 0.2 (see equation (1)). For this set of values, the tuning parameters ε and A that fit the points depicted in Figure 9a,b are ε = 0.07 and A = 20. A comparison between the predicted and observed values for large gap ratios is depicted in Figure 13.

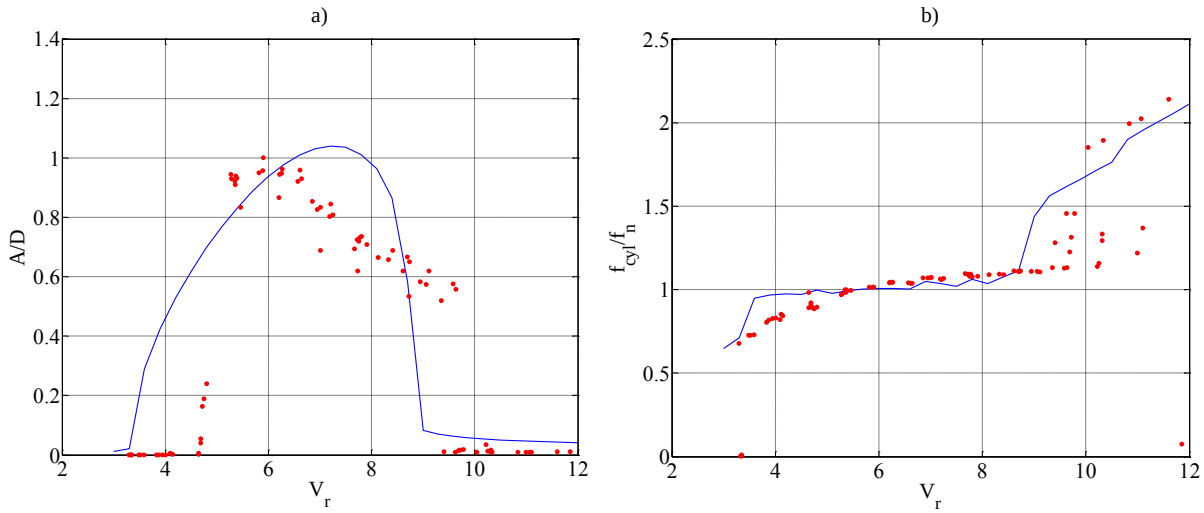

Figure 13. a) amplitude of oscillations; b) frequency of oscillations. Blue line = system of equations (15); red dots = experiments ($G > 2D$)

Differences can be seen between the predicted and observed responses. For example, when compared to the experimental results, the wake oscillator model predicts a smaller flow velocity for the beginning of lock-in, and a higher flow velocity for the maximum deflection of the cylinder. Additionally, the empirical model predicts a more gradual increase of oscillations after the start of lock-in and a quick attenuation of oscillations after the maximum deflection is reached, while the experiments reveal an abrupt increase of oscillations shortly after the lock-in starts ($V_r = 5$) and a smoother decrease of oscillations after the maximum amplitude is reached (lower branch). Despite these differences, the main characteristic of the response is captured, namely a lock-in region where oscillations are amplified. Also, the amplitude of oscillations are of the same order, and the frequencies follow closely the observed ones.

For this scenario in which the cylinder is constrained to move solely in the vertical direction ($u_x = 0$), the in-line force is calculated with

$$F_x = \frac{1}{2}\rho_w D\left[C_{D0}V\cos\alpha - \frac{q}{2}C_{L0}\left(V\sin\alpha - \dot{u}_z\right)\right]U \tag{16}$$

The in-line coefficients $\bar{C}_x$ and C_{x2} and the phase angle ϕ_2 (cf. section 4) calculated based on the forces predicted by equation (16) and calculated based on the forces measured during the free vibration experiments are compared in Figure 14. As can be observed, the wake oscillator model suggests an amplification of in-line force coefficients during lock-in, but with a different dependence on the reduced velocity (amplitudes and shape of curves).

More accurate dependencies of the in-line coefficients on the reduced velocity can be simulated if different tuning parameters are used, but at the expense of deteriorating the fitting of the cross-flow displacements. For instance, if the set $\varepsilon = 0.04$ and $A = 15$ is used, the mean coefficient $\bar{C}_x$ will assume a maximum value around 3 and the coefficient C_{x2} will follow the points depicted in Figure 14b very closely. However, for that set of tuning parameters, desynchronization (end of lock-in) will happen at $V_r = 7.5$, and thus the predicted cross-flow displacements will not account for the oscillations observed in the lower branch.

In fact, by adjusting the tuning parameters, one can approximate certain features of the response better. For example, in trying to reproduce the results obtained by Khalak et al. [7] (different damping and different mass), Ogink and Metrikine [12] suggested that $\varepsilon = 0.05$ and $A = 4.0$ represent well the upper branch of the lock-in region, while $\varepsilon = 0.7$ and $A = 12.0$ represent the lower branch better. Approximating one feature thus results in the deterioration of other features, and so a compromise must be reached. In the remainder of this work, the set $\varepsilon = 0.07$ and $A = 20$ is used, which, in the authors' opinion, is the one that better approximates the cross-flow displacements measured in the current experiments for a wide range of velocities.

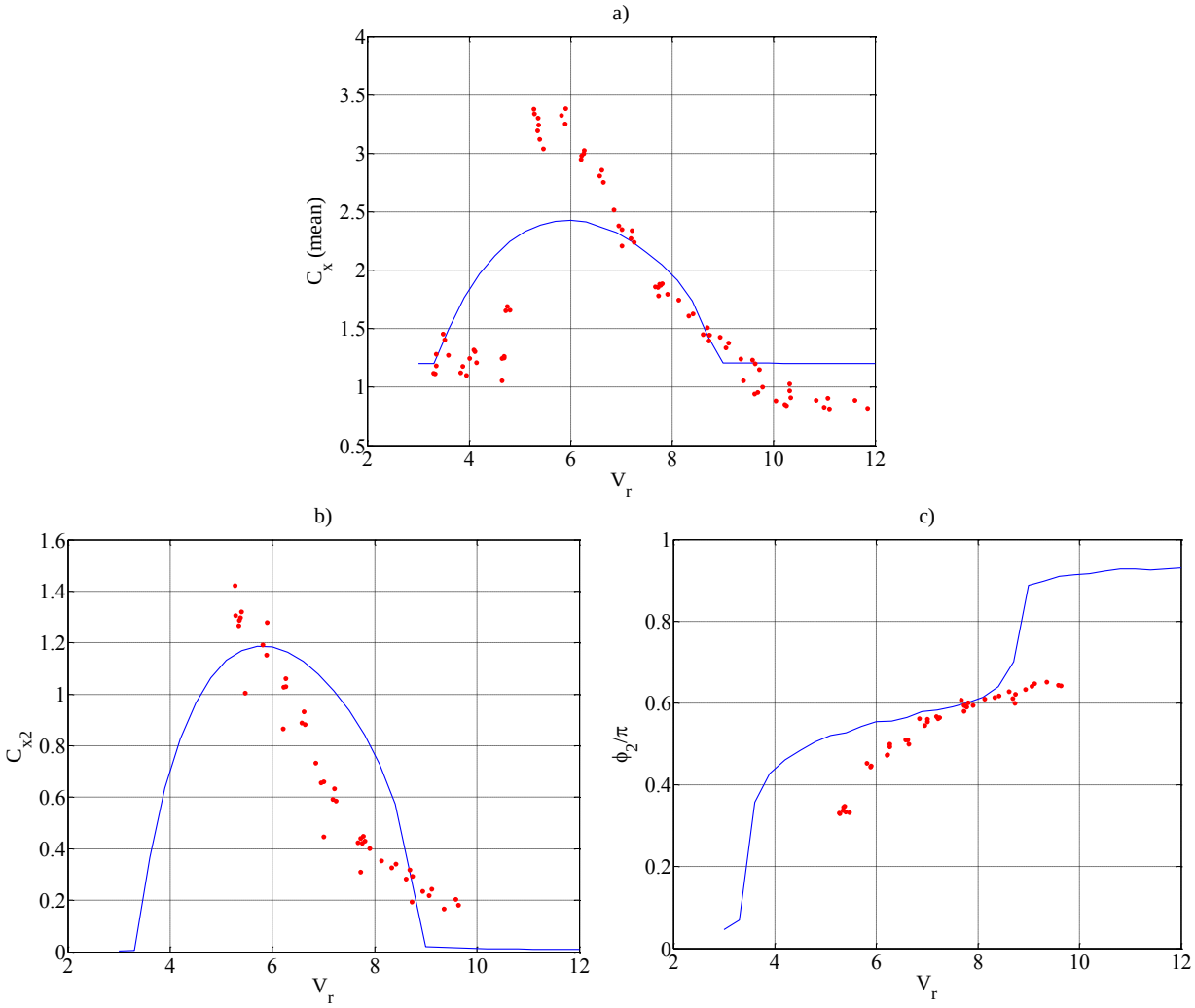

Figure 14. a) mean in-line force coefficient $\bar{C}_x$; b) in-line force coefficient C_{x2}; c) Phase ϕ_2. Blue line = system of equations (15); red dots = experiments ($G > 2D$)

5.2. Enhancement of the model

The free vibration experiments revealed that the presence of a boundary affects the response of the cylindrical system in two ways: first, by reducing the amplitude of the oscillations as the cylinder is placed closer to the bottom; second, by introducing a maximum value for the downward deflection (impact). These two aspects should be incorporated in the empirical model described above if more rigorous predictions are desired for structures lying on the seabed.

The reduction of amplitudes has been explained as a result of a vertical force that opposes the motion of the cylinder, i.e., a force which acts upward when the cylinder moves down, and downwards when the cylinder moves up. This force F_{BP} (BP standing for boundary proximity), which acts only when the bottom of the cylinder is close enough to the boundary, e.g., for distances shorter than κD, can be written as

$$F_{\mathrm{BP}} = -\frac{1}{2}\rho_w D C_{\mathrm{BP}} U\, \dot{u}_z\, \mathrm{H}(\kappa D - u_z - G) \tag{17}$$

where G is the gap between the bottom of cylinder (at rest) and the plane boundary, H(…) is the Heaviside function, and C_{BP} is a dimensionless force coefficient (similar to C_{D0} and C_{L0}). After adding the force F_{BP} to the right hand side of the second line of the system of equations (15), and setting $\alpha = 0$, one obtains

$$(m + m_a)\ddot{u}_z + c_z\dot{u}_z + k_z u_z = \frac{1}{2}\rho_w D\left[-\left(C_{D0} + C_{\mathrm{BP}}\mathrm{H}(\kappa D - u_z - G)\right)\dot{u}_z + \frac{q}{2}C_{L0}\left(V - \dot{u}_x\right)\right]U \tag{18}$$

The parameter κ and the force coefficient C_{BP} have to be tuned in order to fit the response obtained experimentally. Based on the experimental results, where it is observed that for $G>2D$ there is no influence of the bottom and that for these gaps the amplitude of oscillations is around $A=1D$, the value $\kappa=1$ appears to be a good choice. For $\kappa=1$, and keeping ε and A unchanged, the value of C_{BP} that provides the best fit of the experimental amplitudes is $C_{BP}=0.4$. The observed and predicted oscillations for the gap ratios $G/D=\{1.5,1,0.75\}$ are compared in Figure 15.

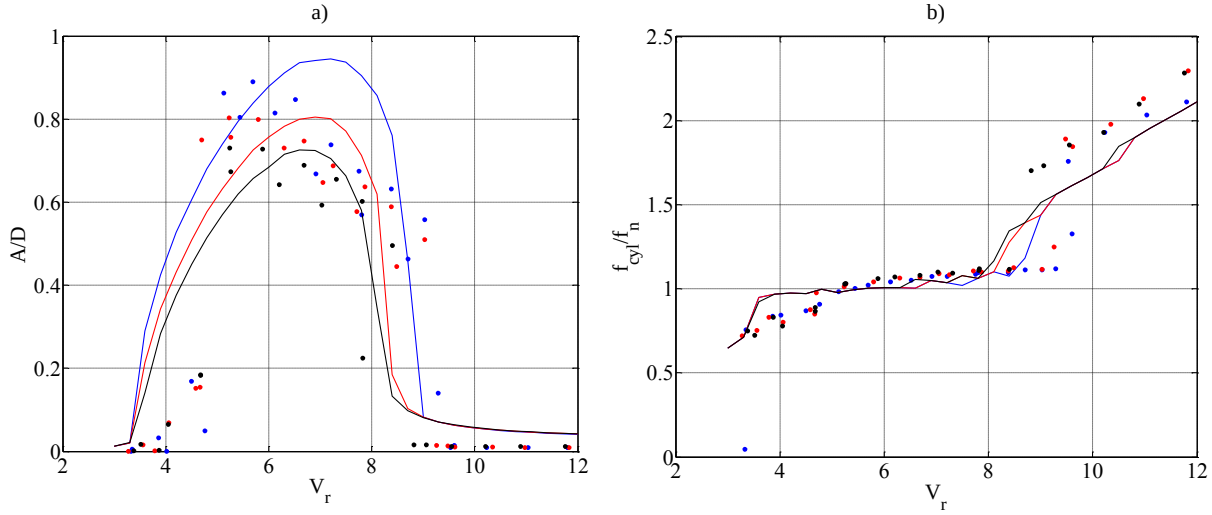

Figure 15. a) amplitude of oscillations; b) frequency of oscillations. Gap ratio (G/D) = 1.5 (blue), 1.0 (red), and 0.75 (black). Solid lines = predicted values; dots = experimental results. (For interpretation of the references to colour in this figure legend, the reader is referred to the web version of this article.)

The differences between the predicted and observed responses are the same as shown in Figure 13 (wider lock-in region, smoother transition to upper branch, and shaper drop of oscillations). Nevertheless, the maximum deflections decrease as the cylinder is placed closer to the bottom (smaller gaps), which verifies that the vertical force expressed in equation (17) can indeed reproduce the effect of the proximity of the boundary.

The second aspect associated with the boundary proximity (the impact of the cylinder on the bottom) can be simulated with springs k_B and dashpots c_B that are activated only when the cylinder reaches the boundary when ($u_z+G<0$). Equation (18) is therefore rewritten as

$$\begin{aligned}\left(m+m_a\right)\ddot{u}_z+\left[c_z+c_B\mathrm{H}\left(-u_z-G\right)\right]\dot{u}_z+k_zu_z+k_B\mathrm{H}\left(-u_z-G\right)\left(u_z+G\right)=\\ \frac{1}{2}\rho_wD\left[-\left(C_{D0}+C_{BP}\mathrm{H}\left(\kappa D-u_z-G\right)\right)\dot{u}_z+\frac{q}{2}C_{L0}\left(V-\dot{u}_x\right)\right]U\end{aligned} \tag{19}$$

The term $\left(u_z+G\right)$ represents the penetration of the cylinder in the boundary.

The springs k_B must be representative of the rigidity of the boundary, while the dashpots c_B must be representative of the energy that is dissipated during the impact. For the reproduction of the experimental conditions, the values $k_B=100\,k_z$ (rigid bottom) and $c_B=25\,c_z$ (best fit) are used. Figure 16 compares the predicted and registered upward deflections for the cases in which impact is observed, i.e., $G/D=\{0.5,0.25,0\}$. It can be observed that the main characteristics of the response are captured: higher oscillating frequencies and upward deflections for faster flows; desychronization at higher flow velocities for smaller gaps; higher frequency for shorter gaps. In general, the predicted amplitudes are higher than the registered ones, and the difference increases as the gap decreases. Based on the relatively good match, it is admissible to conclude that the inclusion of proper bottom springs k_B and bottom dashpots c_B can provide good predictions for the cases in which impact occurs.

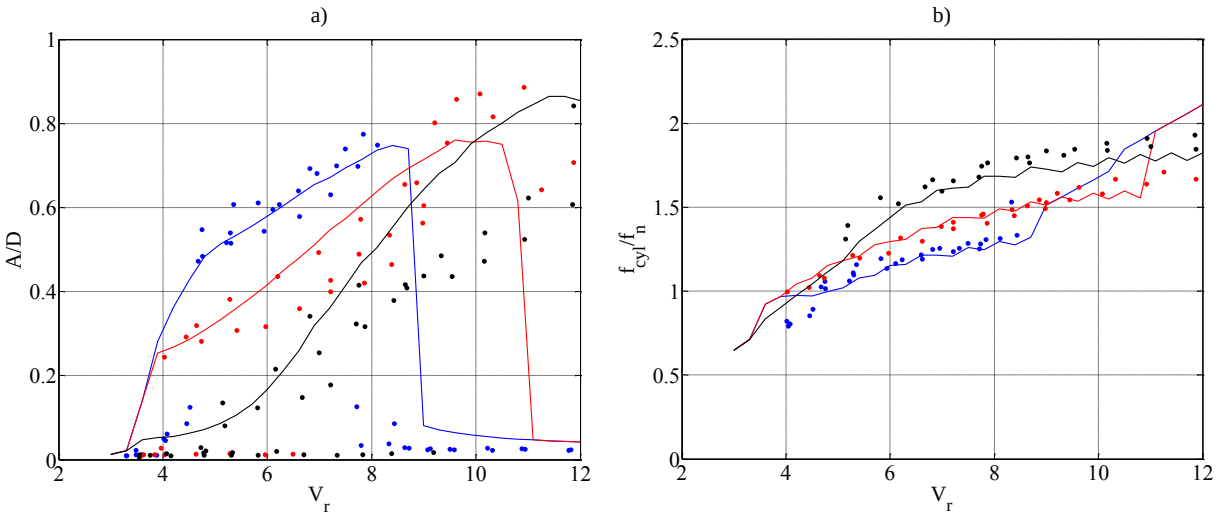

Figure 16. a) upward deflection; b) frequency of oscillations. Gap ratio (G/D) = 0.5 (blue), 0.25 (red), and 0.0 (black). Solid lines = predicted values; dots = experimental results. (For interpretation of the references to colour in this figure legend, the reader is referred to the web version of this article.)

6. Conclusions

This work focussed on the response of cylindrical structures exposed to steady currents and located near a plane boundary. The problem was investigated experimentally through stationary and free-vibration measurements with cylinders placed at varying distances from the bottom of the flume. Based on the observed dynamics, the existing wake oscillator model for vortex-induced vibration was extended to incorporate effects related to the proximity of a plane boundary.

The features observed in the stationary experiments are consistent with previously reported results by other authors. The results obtained in the free vibration measurements allowed a number of conclusions to be drawn about the vertical response of the cylinder and the acting in-line forces. Regarding the vertical response, it was observed that inside the lock-in region, the amplitude of oscillation is not affected by the plane boundary if the gap between the cylinder and the boundary is larger than two diameters. For gaps between 0.75 and 2 diameters, the amplitude of oscillations tend to decrease, but the oscillations remain symmetric with respect to the equilibrium position, and no impact with the boundary is observed. For gaps smaller than 0.75 diameters, the cylinder will impact the boundary, resulting in a non-symmetric oscillation. Also, the lock-in region widens (with respect to the previous two cases), and the upward displacement and the frequency of oscillation tend to increase as the flow velocity is increased.

As for the in-line forces, it is observed that these are amplified inside the lock-in region, and can reach values as high as three times the corresponding stationary force. Also, two oscillating components of the in-line force are observed, one characterized by the same frequency as the vertical oscillation of the cylinder, and the other by twice that frequency. For gaps smaller than two diameters, the magnitude of the first component tends to increase with decreasing gap, while the magnitude of the second tends to decrease in the same amount.

The modifications to the existing wake-oscillator model aimed at incorporating the above mentioned gap-dependencies, namely the ones related to the vertical response of the cylinder. The first addition is a piecewise damper, which accounts for the decrease of amplitudes associated with the cylinder approaching the boundary. This damper is activated only when the cylinder reaches a certain distance from the boundary. The second addition is a piecewise spring-damper couple, which accounts for the stiffness of the boundary and the energy dissipation during impact. Like the first damper, this couple is only activated when the cylinder reaches the boundary position. The comparison between the predicted and observed results allowed to conclude that these modifications capture very well the alterations in the cylinder response due to the proximity of a boundary.

Acknowledgments

This work has been sponsored by the program FLOW (Far and Large Offshore Wind – flow-offshore.nl), under the theme “Wind Farm Design” and research project “Optimizing cable installation and operation, a life cycle perspective” (project code: P201305-004-IHC).

References

1. G. Schewe. On the force fluctuations acting on a circular cylinder in crossflow from subcritical up to transcritical Reynolds numbers. Journal of Fluid Mechanics, Volume 133, pp 265-285, 1983
2. R. Gopalkrishnan. Vortex-induced forces on oscillating bluff cylinders, PhD thesis, Department of Ocean Engineering (MIT) and Department of Applied Ocean Physics and Engineering (WHOI), 1993
3. Hover, F. S., A. H. Techet, and M. S. Triantafyllou. Forces on oscillating uniform and tapered cylinders in cross flow. Journal of Fluid Mechanics, Volume 363, pp 97-114, 1998
4. O.M. Griffin and G.H. Koopmann. The vortex-excited lift and reaction forces on resonantly vibrating cylinders. Journal of Sound and Vibration, Volume 54, Issue 3, pp 435-448, 1977
5. A. Khalak and C.H.K. Williamson. Dynamics of a hydroelastic cylinder with low mass and damping. Journal of Fluids and Structures, Volume 10, Issue 5, pp 455-472, 1996
6. A. Khalak and C.H.K. Williamson, Fluid forces and dynamics of a hydroelastic structure with very low mass and damping. Journal of Fluids and Structures, Volume 11, Issue 8, pp 973-982, 1997
7. A. Khalak and C.H.K. Williamson. Motions, forces and mode transitions in vortex-induced vibrations at low mass-damping. Journal of Fluids and Structures, Volume 13, Issues 7–8, pages 813-851, 1999
8. Govardhan, R., and C. H. K. Williamson. Modes of vortex formation and frequency response of a freely vibrating cylinder. Journal of Fluid Mechanics, Volume 420, pp 85-130, 2000
9. A. Sanchis, G. Sælevik and J. Grue. Two-degree-of-freedom vortex-induced vibrations of a spring-mounted rigid cylinder with low mass ratio. Journal of Fluids and Structures, Volume 24, Issue 6, pp 907-919, 2008
10. Blevins, Robert D., and Charles S. Coughran. Experimental investigation of vortex-induced vibration in one and two dimensions with variable mass, damping, and Reynolds number. Journal of Fluids Engineering, Volume 131, Issue 10, 2009
11. M.L. Facchinetti, E. de Langre and F. Biolley. Coupling of structure and wake oscillators in vortex-induced vibrations. Journal of Fluids and Structures, Volume 19, Issue 2, pp 123-140, 2004
12. R.H.M. Ogink and A.V. Metrikine. A wake oscillator with frequency dependent coupling for the modeling of vortex-induced vibration. Journal of Sound and Vibration, Volume 329, Issue 26, pp 5452-5473, 2010
13. P. W. Bearman and M. M. Zdravkovich, Flow around a circular cylinder near a plane boundary. Journal of Fluid Mechanics, Volume 89, Part 1, pp 33-47, 1978
14. M. Zdravkovich. Forces on a circular cylinder near a plane wall. Applied Ocean Research, Volume 7, Issue 4, pp 197-201, 1985
15. G. Buresti and A. Lanciotti. Mean and fluctuating forces on a circular cylinder in cross-flow near a plane surface. Journal of Wind Engineering and Industrial Aerodynamics, Volume 41, Issues 1–3, pp 639-650, 1992
16. C. Lei, L. Cheng and K. Kavanagh, Re-examination of the effect of a plane boundary on force and vortex shedding of a circular cylinder. Journal of Wind Engineering and Industrial Aerodynamics, Volume 80, Issue 3, pp 263-286, 1999
17. F. Angrilli, S. Bergamaschi and V. Cossalter. Investigation of wall induced modifications to vortex shedding from a circular cylinder. Journal of Fluids Engineering, Volume 104, Issue 4, pp 518-522, 1982
18. A. J. Grass, P. W. J. Raven, R. J. Stuart and J. A. Bray. The influence of boundary layer velocity gradients and bed proximity on vortex shedding from free spanning pipelines. Journal of Energy Resources Technology, Volume 106, Issue 1, pp 70-78, 1984

19. J. Fredsoe. B. M. Sumer, J. Andersen and E. A. Hansen. Transverse vibrations of a cylinder very close to a plane wall. Journal of Offshore Mechanics and Arctic Engineering, Volume 109, Issue 1, pp 52-60, 1987
20. B. M. Sumer, J. Fredsoe, B. L. Jensen and N. Christiansen. Forces on vibrating cylinder near wall in current and waves. Journal of Waterway, Port, Coastal, and Ocean Engineering, Volume 120, Issue 3, pp 233-250, 1994.
21. http://www.scaime.com/en/329/produit/aluminum-single-point-load-cell.html (as seen in April 2, 2015)
22. https://www.schneeberger.com/en/products/slides-and-miniature-tables/frictionless-tables/type-nkl/ (as seen in April 2, 2015)
23. http://www.micro-epsilon.com/download/manuals/man--optoNCDT-1302--en.pdf (as seen in April 2, 2015)
24. http://www.industriele-veren.nl/online-shop/trekveren/trekveren-roestvrij-staal-serie-a-b (as seen in April 2, 2015)
25. B. M. Sumer and J. Fredsoe. Hydrodynamics around cylindrical structures (Advanced Series on Ocean Engineering – Volume 26), World Scientific Publishing Co. Pte. Ltd., Singapore, 2006